ACS APPLIED MATERIALS & INTERFACES

Research Article

www.acsami.org

Electron Transport in Acceptor-Sensitized Polymer–Oxide Solar Cells: The Importance of Surface Dipoles and Electron Cascade Effects

Seare A. Berhe,[†] Joy Y. Zhou,[‡] Keith M. Haynes,[†] Marco T. Rodriguez,[†] and W. Justin Youngblood*[,†]

[†]Department of Chemistry, University of North Texas, Denton, Texas 76203, United States

[‡]Department of Chemistry, University of Minnesota, Minneapolis, Minnesota 55455, United States

Supporting Information

ABSTRACT: Fullerene and acenequinone compounds have been examined as electron mediators between a p-type semiconductive polymer and two n-type oxide semiconductors. Composite interlayer materials and photovoltaic test cells were assembled and studied for their fluorescence quenching, current–voltage, and quantum efficiency behavior to characterize the efficacy of the acceptor-sensitizers as electron-selective interlayers. The sensitizers are generally more effective with titanium dioxide than with zinc oxide, due to the difference in magnitude of dipole-induced vacuum level shifts at the respective oxide interfaces. In titanium dioxide-based solar cells, where dipole effects are weak, photovoltage and fill factor increase in a trend that matches the increase in the first reduction potential of the acceptor-sensitizers. Photosensitization of the oxide semiconductor by the acceptor-sensitizers is observed to operate either in parallel with the polymer as an alternate photosensitizer or in series with the polymer in a two-photon process, according to an acceptor-sensitizer's first reduction potential. In zinc oxide-based solar cells, where dipole effects are stronger, the acceptor-sensitizers impaired most devices, which is attributed to an upward shift of the oxide's conduction band edge caused by dipole-induced vacuum level shifts. These results have broad implications for designing electron-selective interlayers and solid-state photocells using sensitized oxide semiconductors.

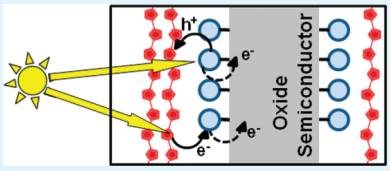

KEYWORDS: *electron, acceptor, sensitizer, polymer, oxide, nanorods, organic, photovoltaic*

INTRODUCTION

Hybrid inverted solar cells that employ metal oxide semiconductors such as titanium dioxide (TiO_2) and zinc oxide (ZnO) with organic semiconductive polymers have been investigated for several years now as an alternative to all-organic bulk heterojunction composites (Figure 1).[1−9] The oxide semiconductors serve the role of the n-type semiconductor component paired with p-type semiconductive polymers such as poly(3-hexylthiophene) (P3HT) and various poly(phenylenevinylene) and polyfluorene derivatives. The appeal of substituting the oxide semiconductor for an organic acceptor is in the ease and/or reliability of nanostructuring the donor–acceptor interface, as well as in the superior conductivity of the oxide semiconductor relative to an organic semiconductor. Despite these advantages, hybrid inverted solar cells have yet to equal, let alone surpass, the performance of all-organic bulk heterojuction devices. The shortcoming of these hybrid composites is the inferior efficiency of interfacial electron transport at the donor–acceptor interface when the acceptor is an oxide semiconductor. Electron transfer at the P3HT-TiO_2 interface, for example, has been separately examined by photoluminescence quenching and time-resolved microwave conductivity (TRMC)[10,11] and found to be poorly efficient. In P3HT-$Zn_{1-x}Mg_xO$ composites, TRMC analysis has shown that most photogenerated charge carriers form within the P3HT bulk rather than at the interface, and must transfer as free carriers into the oxide acceptor.[12] The yield of free photogenerated charge carriers within P3HT and other p-type semiconductive polymers upon illumination is not high, so

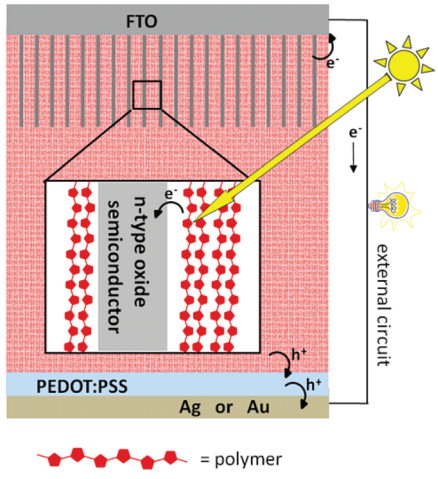

Figure 1. Electron transport events in polymer-oxide excitonic solar cells.

Received: February 17, 2012
Accepted: May 9, 2012
Published: May 9, 2012

fullerene acceptors including C60 and [60]PCBM are commonly blended into the polymer component to increase the photocurrent yield, creating a donor–acceptor–acceptor electron cascade with at least three possible electron transfer interfaces: polymer–oxide, polymer–fullerene, and fullerene–oxide.[6,13–17]

More recent studies have substituted or complemented the bulk fullerene acceptor by placing fullerenes directly at the polymer–oxide interface.[18–23] Other interfacial modifiers, including ruthenium–polypyridyl, zinc porphyrin, and other dyes,[18,24–28] as well as other aromatic and aliphatic molecular species, have been explored to varying degrees of electron transfer enhancement.[20,25,26,29] None of these interfacial modifiers match the photocurrent boost from blending fullerenes into the polymer bulk, and not all are intended to create an electron cascade. Other factors cited for the benefits of molecular interfacial modifiers are: (1) providing a low-dielectric interface environment that improves the wettability of the oxide component by the polymer[24,26] or alters the polymer chain packing near the oxide surface,[29] (2) lowering the conduction band edge by interface dipoles of carboxylate binding groups and/or the overall molecular dipole of the molecular modifier,[30–32] (3) photosensitizing the oxide with the molecular monolayer and thermally transferring holes into the polymer,[27,28] and (4) inhibiting back electron transfer (recombination) from the oxide conduction band to the polymer.[24,26]

We have investigated the importance of an electron transport cascade at interfacially modified P3HT-oxide semiconductor junctions by examining a set of acceptor-sensitizers (Chart1)

Chart 1. Acceptor-Sensitizers Investigated in This Study[a]

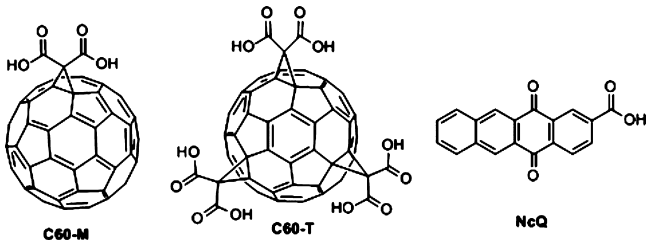

[a]**C60-M** = monoadduct [60]fullerene. **C60-T** = trisadduct [60]-fullerene. **NcQ** = naphthacenequinone.

having increasingly negative first reduction potentials at interfaces of P3HT with ZnO and TiO_2 nanorod films. For interfaces of pristine polymer with oxide semiconductors, we propose that an increase in reduction potential of the intermediate acceptor-sensitizer should provide greater over-potential for electron transfer into the oxide (Figure 2), possibly boosting photovoltaic performance. As a tunneling barrier against recombination at the oxide interface, such sensitizers can in principle be helpful even for devices using a P3HT/PCBM blend, wherein the electron cascade is not expected. These electron cascade effects should be observable when dipole-induced vacuum level shifts are minimal, but will be muted when dipole effects are stronger.

We found that the use of these interfacial monolayers is helpful with TiO_2, regardless of whether PCBM is included or omitted in a given device. In contrast, when P3HT/PCBM blends were used with ZnO, the acceptor-sensitizers severely reduced the photocurrent and photovoltage, although some devices without PCBM were enhanced by sensitization.

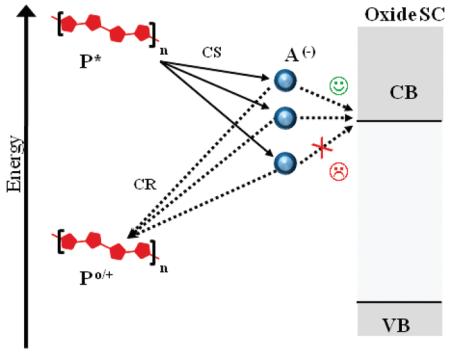

Figure 2. Qualitative view of energetic considerations of electron transport at polymer-sensitizer-oxide interfaces. Solid lines indicate photoinduced electron transport. Dotted lines indicate dark (thermal) electron transport. CS = charge separation. CR = charge recombination. CB = conduction band. VB = valence band. SC = semiconductor.

Photosensitization by some of the acceptor-sensitizers was apparent at P3HT-TiO_2 interfaces, despite insufficient energetics for electron transfer from neutral photoexcited acceptor molecules to the oxide. We propose that this photocurrent generation could arise from hole transfer from photoexcited acceptors to P3HT, leading to dark (thermal) electron injection into the oxide semiconductors by the resulting radical anion acceptor-sensitizers.

RESULTS AND DISCUSSION

Selection of the Acceptor-Sensitizers. We chose the easily prepared **C60-M** (Figure 2) as the benchmark acceptor-sensitizer because various monoadduct fullerenes have already been reported to enhance charge transfer at interfaces between P3HT and either ZnO or TiO_2.[18–21] Additional molecular acceptor compounds include an e,e,e-trisadduct fullerene (**C60-T**), and a naphthacenequinone (**NcQ**). The equatorial placement of malonic acids on the trisadduct **C60-T** was chosen to enable a most-stable tridentate binding configuration at the oxide surface. Table 1 shows the redox potentials, in descending order, for the neutral excited and/or radical anion

Table 1. Redox Potentials of Organic Semiconductors and Conduction Band Edges of ZnO and TiO_2[a]

substance	ESOP$^{(*/+)}$	RP$^{(-)}$/CBE	ref
P3HT (dry)	−1.95[b]		36
P3HT	−1.10		37,38
NcQ	^{S}−1.08/^{T}−0.57[c]	−1.13[d,e]	39
C60-T	^{S}−0.44/^{T}−0.17	−0.86[e]	40
PCBM	^{S}−0.29/^{T}−0.01	−0.67[d]	41,42
PCBM (dry)	^{S}−0.61/^{T}−0.4[b]	−0.9[f]/−0.4[g]	36,42–44
C60-M	^{S}−0.2/^{T}0.1	−0.64[e]	40,42,45
ZnO (dry)		−0.60[g]	6
TiO_2 (dry)		−0.5[g]/−0.25[g]	32,46

[a]All potentials determined for solvated species vs. SCE or converted to SCE from other electrodes[47] or vacuum level,[48] where indicated. ESOP = excited state oxidation potential. RP = reduction potential. CBE = Conduction Band Edge. ^{S}Singlet excited state. ^{T}Triplet excited state. [b]Originally reported vs vacuum (UPS). [c]Reported for 5,12-naphthacenequinone. [d]Originally reported vs ferrocene couple. [e]Measured from ester derivative. [f]Originally reported vs vacuum (IPES). [g]Originally reported vs vacuum (Kelvin probe).

dx.doi.org/10.1021/am300282d | ACS Appl. Mater. Interfaces 2012, 4, 2955–2963

Scheme 1. Synthesis of C60-T from Commercially Available Starting Materials

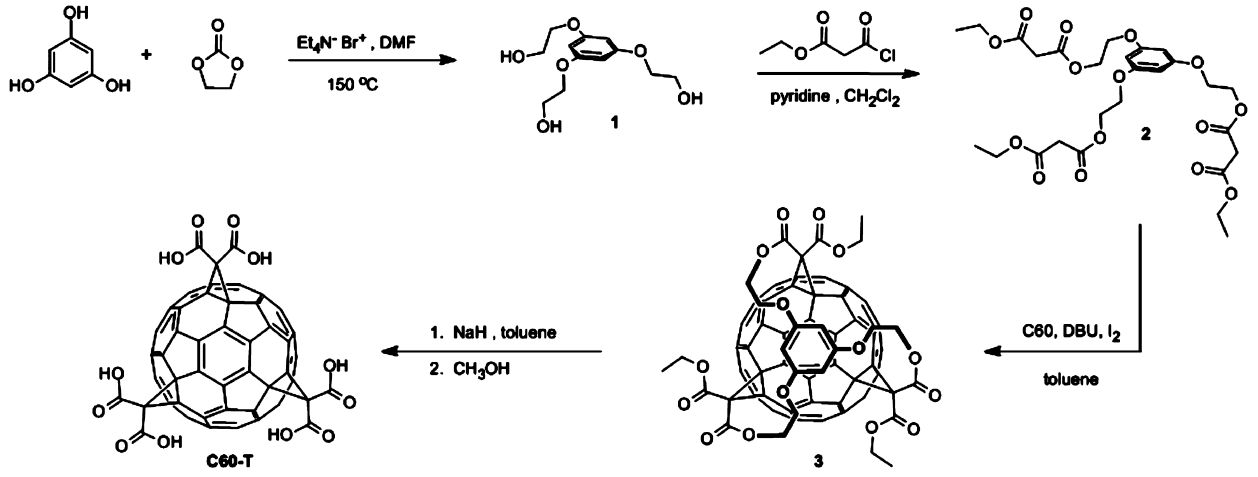

Scheme 2. Synthesis of NcQ from Commercially Available Starting Materials

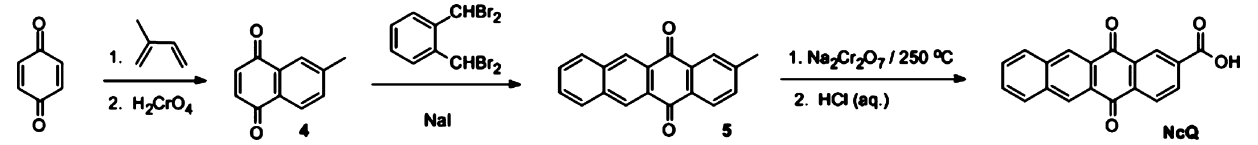

states for P3HT and all the acceptor species examined in this study, along with the band edge potentials for ZnO and TiO_2 as measured in air. The excited state oxidation potential (ESOP) is determined via the ground state oxidation potential (E_{ox}) and the excited state energy (E_{0-0}) by eq 1:

$$\text{ESOP} = E_{ox} - E_{0-0} \quad (1)$$

An important caveat for the table is that the Kelvin probe data are reported for anatase TiO_2, whereas the TiO_2 nanorods we employ in this study are rutile.[33] Although the conduction band edge of rutile TiO_2 is reported to be 200 mV positive of the band edge of anatase TiO_2 in the presence of electrolyte,[34] no corresponding offset has been reported in dry conditions. We could find no literature report for a Kelvin probe measurement of undoped rutile TiO_2 at the time of preparing this manuscript, however we note that a reported measurement is available for rutile TiO_2 doped with 0.05 wt % Nb, placing the band edge at 4.2 eV below vacuum for the [110] crystal face,[35] which is the operative surface of the TiO_2 nanorods as grown for this study.[33]

Voltammetrically-determined redox potentials for dissolved polymeric and molecular semiconductors are commonly converted to the vacuum scale and assumed to be relevant to the solventless environment of solid-state material composites such as bulk heterojunctions and hybrid excitonic solar cells. Unfortunately, reported redox measurements for dry photoelectroactive compounds by methods such as Kelvin probe contact potential, ultraviolet photoelectron spectroscopy (UPS), and inverse photoemission spectroscopy (IPES) do not consistently agree with one another or with values obtained by liquid phase voltammetry. For example, Kelvin probe measurement of the energy level for PCBM radical anion (−0.4 V vs SCE) places the species at lower energy than gauged by cyclic voltammetry in solution (−0.67 V vs SCE), which is lower still than that determined from IPES (−0.9 V vs SCE). There is a need for a clearer understanding of whether and how the redox potentials of polymeric and molecular semiconductors may shift from a solvated to solventless environment. For this study, we have relied on the assumption that the acceptor-sensitizers must be all affected in a uniform manner, such that the hierarchy of first reduction potentials of these compounds in solution will be maintained in solid-state films.

Synthesis of the Acceptor-Sensitizers. Preparation of the C3-symmetric **C60-T** was adapted from a reported synthesis of such equatorial (*e*,*e*,*e*)-trisadduct fullerenes by Hirsch and co-workers (Scheme 1).[49] Compound **NcQ** has been previously reported starting from 1,4-anthraquinone,[50] but that synthesis requires a laborious preparation of the unstable precursor 2-hydroxymethyl-1,3-butadiene.[51] We devised a shorter, easier route through the fusion of methylnaphthoquinone and $\alpha,\alpha,\alpha',\alpha'$-tetrabromoxylene. The resulting methylnaphthoquinone **5** is oxidized to the corresponding carboxylic acid **NcQ** without damaging the quinoidal keto groups by the use of $Na_2Cr_2O_7$ under forcing conditions.[52]

Growth of Nanostructured Oxide Materials. We prepared ZnO nanorod films following the seeding method by Ohyama and co-workers,[53] and using a modification of the growth conditions reported by Hodes and co-workers.[54] Nanorods of ∼50 nm diameter were grown to 300 nm height (see Figure S1 in the Supporting Information). This height is sufficient to achieve near-opacity in the region of the visible spectrum where the polymer absorbs (400−600 nm), and thickness is otherwise minimized to compensate for the weak charge carrier mobility in the polymer. P3HT films that are thicker than ∼300 nm experience greater series resistance due to the conductivity of charge carriers being inferior in organic semiconductors compared to inorganic semiconductors. TiO_2 (rutile) nanorods were grown using the hydrothermal method reported by Liu and Aydil (see Figure S2 in the Supporting Information).[33] We observed a ∼90 min induction period for nanorod growth, after which the growth is rapid. Achieving short nanorod films of reproducible height requires careful timing. Because these TiO_2 nanorods are thicker (∼100 nm diameter), their surface area enhancement relative to a planar

surface is minimal. Taller nanorod films give better surface area for the electron transfer interface, but incur the series resistance of the poorly conductive polymer. A film height of ~750 nm was found to give the best current–voltage behavior for unsensitized TiO_2. Shorter films (200 nm) exhibited much lower photovoltages. Further work in this direction is in progress to control the growth at short film heights and narrow the nanorod diameter, but was not crucial to this study.

Assembly of Hybrid Inverted Organic Solar Cells. Durrant and co-workers showed that short-circuiting of hybrid inverted OPVs could be prevented by blocking the electron recombination at the interface where P3HT meets the conductive oxide substrate.[5] We prepared TiO_2 underlayer films by thermal evaporation of titanium metal to 100 Å thickness, followed by annealing of the Ti film to 450 °C under ambient atmosphere. Upon annealing, the translucent gray Ti film becomes a clear, colorless TiO_2 film of ~10 nm thickness as measured by profilometry. This electron-selective interface has only a mild effect on the resulting solar cell output, exhibiting a slight increase in photovoltage (see Figure S3 in the Supporting Information), but its consistent use prevents the assembly of short-circuited devices, whereas without the TiO_2 underlayer we found that a high percentage of devices were shorted. The TiO_2 underlayer also provides a convenient seeding for the growth of rutile nanorods. Further details on the device assembly are available in the Supporting Information.

Fluorescence Quenching and Current–voltage Behavior in Sensitized P3HT-TiO_2 Devices. Steady-state fluorescence quenching studies (Figure 3) show that P3HT

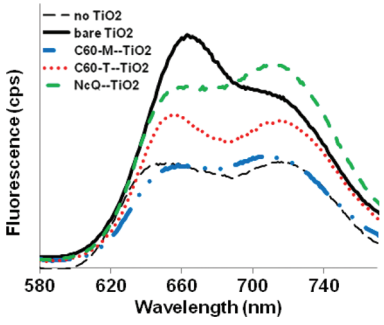

Figure 3. Fluorescence of P3HT as neat film, and on bare and sensitized TiO_2 nanorods.

fluorescence increases when embedded within TiO_2 nanorods, most likely due to the loss of polymer chain crystallization. This indicates that fluorescence quenching due to photoinduced electron transport at the P3HT-TiO_2 interface is weak. Another possible explanation is that a significant amount of P3HT is farther than the exciton diffusion length (~10–20 nm) from the TiO_2 surface. SEM images of the TiO_2 nanorods film (see Figure S2 in the Supporting Information) indicate that the average spacing between nanorods is quite narrow (<50 nm), so we attribute the lack of fluorescence quenching to a poor quantum yield of electron transfer at the polymer-oxide interface. Some quenching is observed between P3HT and acceptor-sensitizer monolayers as the first reduction potential of the sensitizer trends more positive, reflecting an increasing driving force for electron transfer. Subtle differences in the shape of the luminescence peaks may indicate conformational differences in the polymer chain packing induced by the change in wettability at sensitized oxide surfaces relative to bare TiO_2.

Dramatic evidence for altered electron transport behavior is shown in the current–voltage and quantum efficiency behavior of test devices having P3HT-Acceptor-TiO_2 interfaces. Figure 4

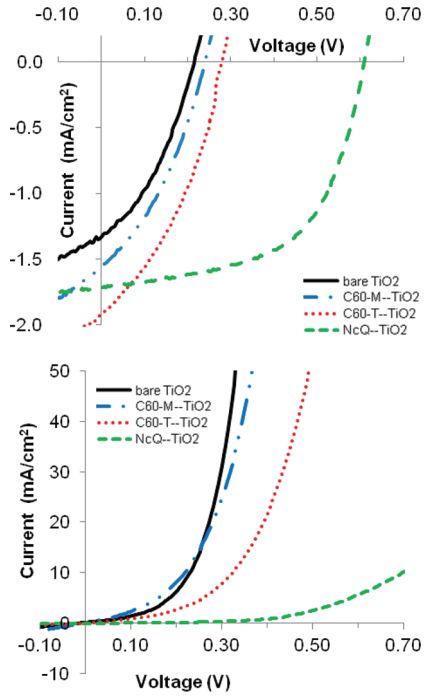

Figure 4. Current–voltage behavior of P3HT-acceptor-TiO_2 devices under 1 sun illumination (upper) and in the dark (lower).

shows that a reduction in dark current for sensitized TiO_2-based devices compared to bare TiO_2, which is usually a good sign that photovoltaic performance will be improved. The acceptor-sensitized cells do show improved photocurrent, photovoltage and fill factor. Photovoltage and fill factor improvements correlate to the rise in the reduction potentials of the acceptor-sensitizers. Table 2 details the photovoltaic performance of these and other cells tested in this study.

Table 2. Photocurrent, Photovoltage, Fill Factor, And Efficiency of Devices Prepared in This Study[a]

TiO_2 surface	J_{SC} (mA/cm^2)	V_{OC} (mV)	FF	PCE (%)
bare-TiO_2	1.34	216	0.36	0.11
C60-M-TiO_2	1.56	241	0.36	0.13
C60-T-TiO_2	1.92	280	0.37	0.20
NcQ-TiO_2	1.72	609	0.56	0.59

[a] J_{SC} = short circuit current density; mA/cm^2 = milliamps per square centimeter; V_{OC} = open circuit voltage; mV = millivolts; FF = fill factor; PCE = power conversion efficiency.

Photoinduced electron transfer across P3HT-Acceptor-TiO_2 interfaces is more efficient than at the binary P3HT-bare TiO_2 interface. The trend in the inhibition of dark current matches the photovoltage improvement, suggesting that the acceptor-sensitizer monolayer is behaving as an electron-selective contact, presumably as a tunneling barrier to electron transport from the TiO_2 conduction band electrons to P3HT. When the reduction potential of the acceptor-sensitizer is well above the conduction band edge (CBE) of the TiO_2, the density of states in the sensitizer monolayer at the energy level of the TiO_2 CBE

may be too low to support tunneling of the oxide-to-P3HT electron transport.

Surface Dipole Effects in Solid-State Sensitized Oxide Materials and Devices. Another factor in interpreting the data in Figure 4 is that surface dipoles may alter the effective local vacuum levels of the P3HT and TiO_2 domains. The dipole effect has been observed and described in dye-sensitized solar cells having liquid electrolyte or solid-state hole conductor as well as for polymer−oxide composites.[25,30,55,56] When an intervening monolayer of molecules can direct a net dipole at the interface, the side at the negative end of the dipole experiences a higher local vacuum level relative to the side at the positive end of the dipole (Figure 5). Local dipoles at

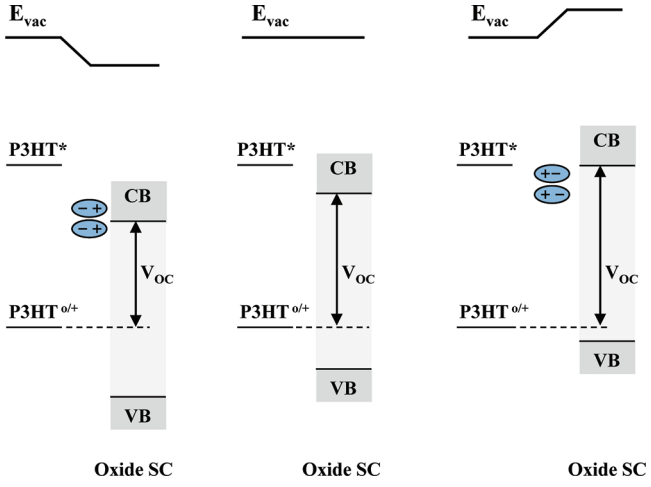

Figure 5. Vacuum level shifts caused by surface dipoles.

carboxylate binding groups will push negative toward the oxide, whereas overall molecular dipoles will vary from one sensitizer to another. The P3HT-acceptor interface may also generate a charge-transfer dipole which would point the negative end toward the oxide surface.[57] The strength of such a dipole would relate to the degree of charge transfer at the interface. When a dipole is positive toward the oxide semiconductor, the vacuum level at the oxide is lowered relative to the polymer phase, with the result that photocurrent increases but photovoltage suffers (Figure 5, left). When a dipole is negative toward the oxide, the vacuum level at the oxide is raised, and photocurrent suffers but photovoltage is boosted (Figure 5, right). The enhancement of one trait (current or voltage) comes at the cost of the other. Dark current trends are also consistent for this paradigm, giving reduced dark current when the oxide semiconductor's vacuum level is raised, and increased dark current when the oxide's vacuum level is lowered. The monolayer is only slightly affected by the shift,[55] and the unbound organic phase remains unmodified from its original vacuum level.[25] The magnitude of the vacuum level shift can be determined according to eq 2:

$$\Delta V = \frac{\mu N_s \cos\theta}{\varepsilon_r \varepsilon_0} \quad (2)$$

In eq 2, ΔV is the magnitude of the vacuum level shift, μ is the surface dipole moment, N_s is the density of dipoles in the surface monolayer, cos θ is the angle of the dipoles from the surface normal, ε_r is the dielectric constant of the medium, and ε_0 is the permittivity of free space. The inverse relation between the local dielectric constant ε_r and the magnitude of the vacuum level shift means that high dielectric oxides like rutile TiO_2 (ε_r = 86)[58] will have much weaker dipole-induced shifts compared to low dielectric oxides like ZnO (ε_r = 8).[59]

DFT calculations for our 3 sensitizers indicate that both fullerenes display dipoles that align roughly parallel to the monolayer (i.e., not directly toward either side of the interface), whereas the **NcQ** sensitizer has a dipole that points the negative end toward the P3HT (see Figure S11 in the Supporting Information). The effects seen for the acceptor-sensitizers in Figure 4 show increased photocurrent and photovoltage, and decreased dark current. These traits do not fit to a dipole effect for a dipole pointing at either side of the interface. We therefore conclude that dipoles are not the dominating effect in the current−voltage behavior of acceptor-sensitized TiO_2 interfaces. The trend of rising first reduction potentials for these sensitizers does fit the pattern of improved photovoltage and fill factor and reduced dark current. The photocurrent enhancement for **NcQ** is less than that for **C60-T**, which may be attributed to weaker driving force for electron transfer at the P3HT-**NcQ** interface, as judged by the lack of fluorescence quenching for the P3HT-**NcQ**-TiO_2 device (Figure 3).

Photosensitization by the Acceptor-Sensitizers. The external efficiency of a solar cell, also known as the IPCE (Incident Photons Converted to Electrons), expresses the efficiency of converting the photon flux into photocurrent at each wavelength according to eq 3:

$$\mathrm{IPCE}(\%) = \frac{1240 J_{sc}}{\lambda P_{in}} \quad (3)$$

J_{SC} and P_{in} represent the photocurrent and the power intensity of the incident light, respectively, at a given wavelength λ. Subtle differences in the ratio of P3HT photosensitization at 500 vs 600 nm in the IPCE spectrum for the P3HT-**NcQ**-TiO_2 and P3HT-bare TiO_2 test cells (Figure 6, top) indicate some conformational difference in the polymer at the bare vs. coated TiO_2 surfaces, in agreement with the fluorescence spectra. For

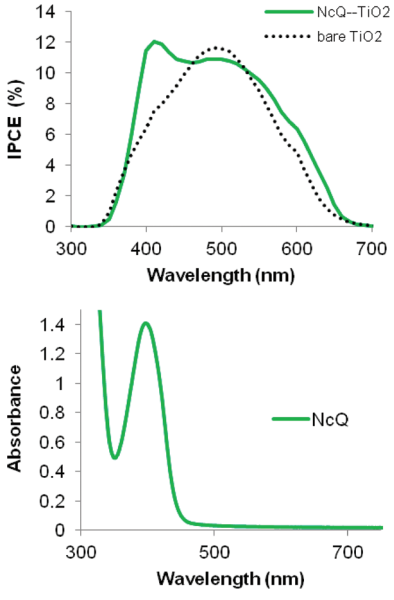

Figure 6. Top: IPCE spectrum of the P3HT-**NcQ**-TiO_2 cell (solid green) overlaid with the P3HT-TiO_2 cell (dotted black); Bottom: Solution-phase UV−vis absorption spectrum for **NcQ** (EtOH).

dx.doi.org/10.1021/am300282d | ACS Appl. Mater. Interfaces 2012, 4, 2955−2963

the **NcQ**-sensitized cell, the peak at ~400 nm indicates photocurrent contribution from light absorption by **NcQ**. Among the acceptor-sensitizers, only the naphthacenequinone (**NcQ**) should have sufficient driving force to donate from either of its neutral excited states (see Table 1; *n.b.*, S^1-T^1 crossover: $k \approx 1 \times 10^{11}$ s^{-1}).[60] Whether the photosensitization by **NcQ** is by donor-quenching (injection by neutral **NcQ*** into TiO_2) or by acceptor-quenching (hole transfer from **NcQ*** to P3HT, followed with electron injection by $\mathbf{NcQ}^-$ into TiO_2) is an important question that can only be definitively answered by transient spectroscopic analysis. Photoexcited naphthacenequinone exhibits rapid acceptor-quenching in the presence of suitable donors.[39,61] Voltammetric oxidation of naphthacenequinone (1.8 V vs SCE) is reported to be irreversible,[62] so a photochemical pathway relying on the formation of $\mathbf{NcQ}^-$ is more likely to lead to a steady-state photocurrent compared to a mechanism relying on the formation of $\mathbf{NcQ}^+$.

Visible light absorption features of both **C60-M** and **C60-T** show broad absorption near 500 nm and strong absorption near 400 nm (see Figure S6 in the Supporting Information). The IPCE spectrum for the P3HT-**C60-T**-TiO_2 cell has a shoulder near 600 nm that matches with the P3HT-only device (Figure 7, upper), but has heightened photocurrent around 400 nm.

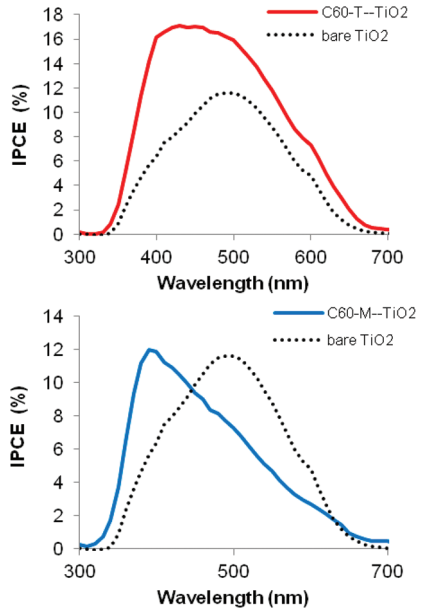

Figure 7. IPCE spectra for P3HT-**C60-T**-TiO_2 cell (top) and P3HT-**C60-M**-TiO_2 cell (bottom). In each spectrum, the dotted trace shows the IPCE for the P3HT-bare TiO_2 cell.

The IPCE spectrum for the P3HT-**C60-M**-TiO_2 cell has a significant peak around 400 nm, and only weak shoulder peaks near 500 and 600 nm that indicate photosensitization by P3HT (Figure 7, lower). Whereas the **C60-T**-device can be interpreted as an overlay of photosensitization by the polymer and acceptor, the IPCE pattern of the **C60-M** device is surprising because the spectrum is dominated by absorption from the acceptor, with substantial loss of photosensitization by P3HT. Although the IPCE trace does not precisely match the UV–vis absorption, we have seen a very similar IPCE spectrum for photosensitization by **C60-M** in NiO-based dye-sensitized solar cells.[63] The significant fluorescence quenching in this TiO_2-based device and enhanced photocurrent relative to the bare-TiO_2 control device suggest that no deficit of charge generation is occurring, but that perhaps the **C60-M** is an inefficient electron mediator due to its lower-lying first reduction potential. We do not know whether the inadequate driving force for charge injection by $\mathbf{C60\text{-}M}^-$ is because the TiO_2 CBE has raised slightly due to a dipole-induced vacuum level shift or because the first reduction potential of **C60-M** in the solventless environment is significantly lower than in solution, or if both factors are operative at this interface.

Effects of the Sensitizers in P3HT/PCBM-TiO_2 Devices. Loss of P3HT-photosensitization is also experienced in the **C60-M** sensitized device using a blend of P3HT/PCBM (Figure 8, upper) along with reduced photocurrent and

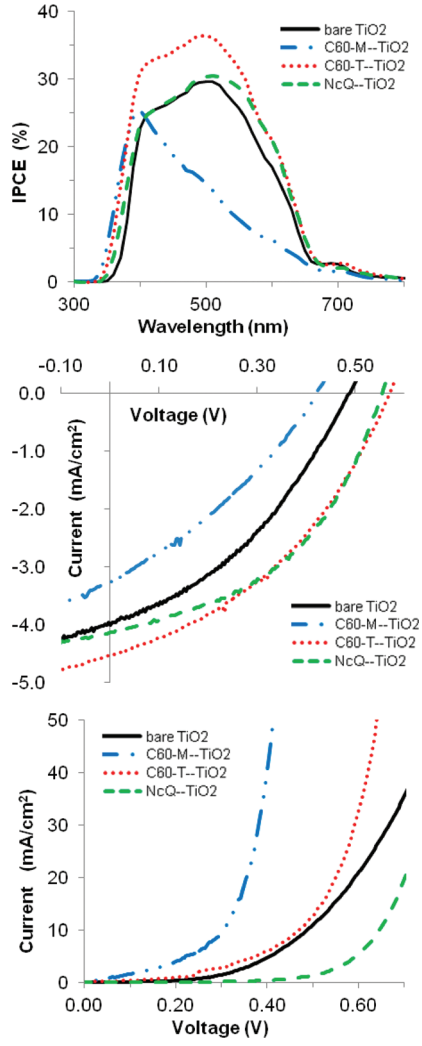

Figure 8. Top: IPCE spectra for [P3HT/PCBM]--Acceptor--TiO_2 devices. Middle and bottom: Current–voltage behavior in [P3HT/PCBM]--Acceptor--TiO_2 devices under 1 sun illumination and in dark, respectively.

increased dark current compared to the control cell with bare TiO_2 (Figure 8, middle and lower). The scale of quantum efficiency is boosted between the two **C60-M**-sensitized devices with/without the PCBM component. Charges generated in the P3HT/PCBM blend must be contributing to photocurrent, but their passage is gated by photosensitization of the **C60-M** monolayer, acting as an electron trap between the P3HT/PCBM blend and the TiO_2. This is Z-scheme photosensitization. Just as a kinetic analysis of a multistep catalytic

cycle would reveal only the slowest process, the quantum efficiency of such a Z-scheme photosensitization will be dominated by the least efficient step. Extending the IPCE analysis into the near-infrared (1200 nm) did not reveal the well-known absorbance peak of the fullerene radical anion at ~1050 nm, but this is due to the dilute illumination of 1 sun intensity: Methods that generate spectroscopically observable fullerene radical anions require either the intense light of a laser pulse (pump–probe spectroscopy) or the voltammetric reduction of a fullerene sample (spectroelectrochemistry). Energy transfer from long-lived fullerene triplet-excited states (100 μs)[42] in the monolayer could provide the second photosensitization to radical anion fullerenes within the monolayer, thereby enabling injection into the TiO_2.

Effects of the Sensitizers on Electron Transport in ZnO Devices. Electron transport mediation by acceptor-sensitizers on ZnO follows a different pattern from that on TiO_2. Two factors responsible for the difference in electron transport behavior at ZnO are the increased role of surface dipole effects at nonpolar ZnO, and a lesser degree of surface coverage by some sensitizers at ZnO. Surface coverage of the ZnO is likely to be incomplete because the sensitization time for coating the ZnO surface must be kept short to avoid etching that occurs at longer soaking times.[64,65] ZnO nanorod films were soaked for just 20 min in baths of the acceptor-sensitizers, compared with overnight soaking for the TiO_2 nanorods. Photoluminescence quenching behavior and dark current of ZnO-based devices were similar to that observed for TiO_2 devices (see Figures S7 and S8 in the Supporting Information), but that is where the similarity between the TiO_2-based and ZnO-based devices ends. For P3HT-only cells, the **C60-T** sensitizer, which is likely to achieve the highest surface coverage due to tridentate binding, exhibits severely reduced photocurrent (Figure 9, upper). The IPCE of the P3HT-**C60-T**-ZnO cell shows photosensitization only from the **C60-T** monolayer. This resembles the Z-scheme photosensitization seen for the **C60-M**-TiO_2 cells (vide infra), suggesting that the ZnO CBE has been raised above the reduction potential of **C60-T**. This is not the first instance of a sensitizer impairing a solid state ZnO device. An earlier report of similar behavior was made by Ackerman and co-workers, who observed photocurrent decline in P3HT-ZnO solar cells wherein the ZnO surface was sensitized with a zinc porphyrin.[27] Careful control over the degree of surface coverage by the sensitizer resulted in the progressive domination of the IPCE behavior by the sensitizer even as the overall quantum efficiency deteriorated along with photocurrent as the sensitizer surface concentration increased. We note also that few solid state ZnO-based dye solar cells have been reported up to the present time and are generally inferior to those based on TiO_2.[66] Among the more successful examples, the deposition of a high dielectric coating over the ZnO nanorods has particularly enhanced such devices. This effect has been assumed to be in forming a tunneling barrier to recombination at the dye–ZnO interface, but we propose that it may also be helping by muting surface dipole-induced vacuum level shifts.

C60-M and **NcQ** show good photocurrent–voltage behavior relative to the control cell with bare ZnO. These sensitizers are likely only partially covering the ZnO, so the extent of dipole-induced vacuum level shift at ZnO should be weaker for these devices given the lower density of dipoles at the surface (eq 2). The result is that P3HT can still inject electrons (at bare areas of the ZnO) even if the acceptor-sensitizers cannot. It is

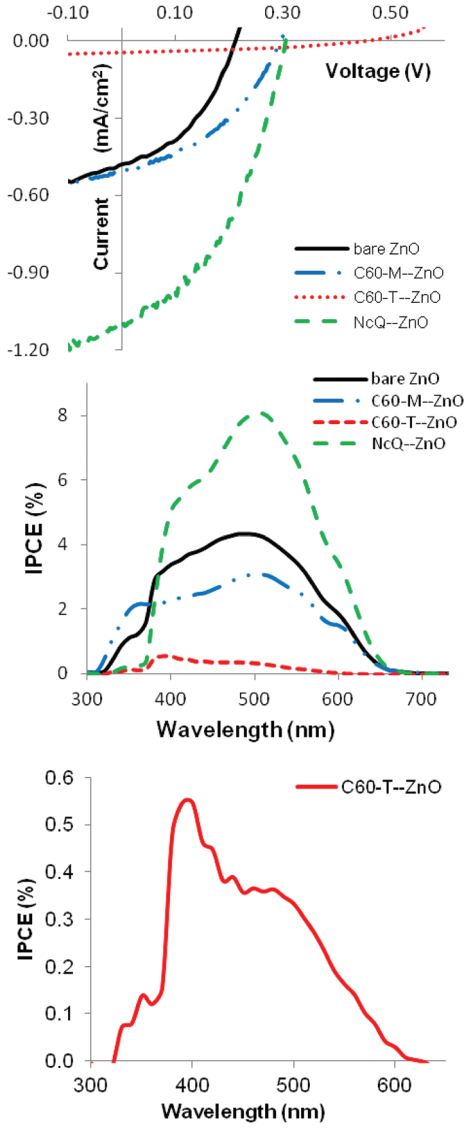

Figure 9. Top: Current–voltage behavior in P3HT-Acceptor-ZnO devices under 1 sun illumination. Middle: IPCE for P3HT-Acceptor-ZnO devices. Bottom: IPCE for P3HT-**C60-T**-ZnO device.

noteworthy that the IPCE spectra for P3HT-**C60-M**-ZnO and P3HT-**NcQ**-ZnO devices show no photosensitization by the acceptor-sensitizers. Photovoltage improvements for these cells are consistent with a raised CBE for ZnO, despite none of the molecular dipoles for the sensitizers having their negative end toward the oxide. It would seem that the local dipoles of the carboxylate groups and/or the charge-transfer dipoles of the P3HT-acceptor interfaces are determining the vacuum level shift. A concomitant loss of photocurrent should accompany the upward shift of CBE, but may be offset by improved wettability of the ZnO surface. Differences in P3HT photosensitization patterns in the IPCE spectra (Figure 9, middle) attest to conformational differences for P3HT in the presence of the acceptor-sensitizer monolayers.

Even partial coverage appears to be a barrier to the P3HT/PCBM blend (Figure 10), as cells with P3HT/PCBM-ZnO composition showed greatly impaired photocurrent for all acceptor-sensitizers. This outcome is a surprising contrast to results reported by other researchers using fullerene monolayers in polymer-ZnO solar cells.[21,23] We interpret the

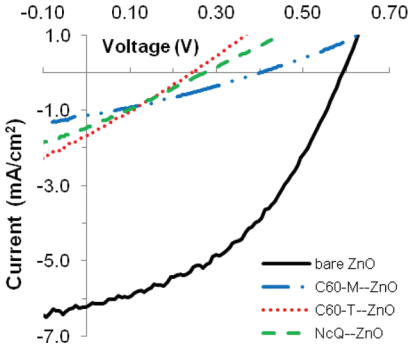

Figure 10. Current–voltage behavior in P3HT/PCBM-Acceptor-ZnO devices under 1 sun illumination.

current–voltage behavior in these cells to indicate that the ZnO CBE is elevated above the reduction potential for PCBM, thereby shutting down electron transfer at the organic–inorganic semiconductor interface. The residual photocurrent shown for each of these devices is quite similar. We suspect that this residual photocurrent arises from interfacial electron transfer at exposed areas of the TiO_2 underlayer employed as a short-circuit barrier in these devices (vide infra). Finally, we note that P3HT-bare ZnO composites gave the highest photocurrent of all devices – this is due to the higher surface area of the P3HT-ZnO interface because the ZnO films have thin, densely packed, well-separated nanorods whereas our TiO_2 nanorods are densely packed but of larger diameter and are partially fused (see Figures S1 and S2 in the Supporting Information). We anticipate that TiO_2 nanorod films with improved morphology and higher surface area will give superior photocurrent, and we are currently exploring methods to produce such films.

CONCLUSIONS

We have determined that acceptor-sensitizers on rutile TiO_2 can provide acceptor-photosensitized charge separation and can act as a recombination barrier between a remote donor component (P3HT) and the TiO_2 conduction band. Although weak vacuum level shifts may be occurring in TiO_2-base devices, such shifts do not appear to significantly affect photovoltaic behavior. The first-reduction potential of the acceptor-sensitizers determines the extent of donor-quenching and the success for electron mediation of transferred electrons arising from donor-sensitization. The photoluminescence quenching of the polymer and apparent trapping of electrons in a monolayer of one sensitizer (**C60-M**) suggest that thermal electron injection by radical anions is an important pathway for charge generation from photoexcited P3HT.

In contrast, ZnO appears to be a less reliable oxide semiconductor for these purposes because of its greater susceptibility to dipole-induced vacuum level shifts. These suggest that the choice of oxide semiconductor for polymer-oxide solar cells and solid state dye-sensitized solar cells must be made with consideration for the sensitivity of less polar semiconductors to interface dipoles of the sensitizing monolayer. In this regard, polar oxides such as rutile TiO_2 (ε = 86),[58] anatase TiO_2 (ε = 50),[67] strontium titanate $SrTiO_3$ (ε = 300)[68], and niobium oxide Nb_2O_5 (ε = 41)[69] will be more resistant to vacuum level shifts compared to SnO_2 (ε = 14)[70] and ZnO (ε = 8).[59] This insight is valuable both for those researchers who may wish to avoid dipole-induced vacuum level shifts and for those who may wish to exploit them.

ASSOCIATED CONTENT

Supporting Information

Figures S1–S7 detailed in the text, as well as spectral data for compound characterization of compounds **2**, **3**, **5**, and **NcQ**. This material is available free of charge via the Internet at http://pubs.acs.org.

AUTHOR INFORMATION

Corresponding Author

*E-mail: youngblood@unt.edu.

Notes

The authors declare no competing financial interest.

ACKNOWLEDGMENTS

We thank the UNT Center for Advanced Research and Technology (CART) for an instrument grant to conduct SEM and profilometry studies, the University of North Texas for startup funding and internal grants (FRG #s GA9550 and GA9154). We thank Prof. Guido Verbeck and AB SciEx for help in obtaining ESI and MALDI mass spectral data, and Prof. Gary Hodes for helpful discussions about the growth of ZnO nanorods films.

REFERENCES

(1) Arango, A. C.; Carter, S. A.; Brock, P. J. *Appl. Phys. Lett.* **1999**, *74*, 1698–1700.
(2) Coakley, K. M.; McGehee, M. D. *Appl. Phys. Lett.* **2003**, *83*, 3380–3382.
(3) Beek, W. J. E.; Wienk, M. M.; Janssen, R. A. J. *Adv. Mater.* **2004**, *16*, 1009–1013.
(4) Beek, W. J. E.; Wienk, M. M.; Janssen, R. A. J. *Adv. Funct. Mater.* **2006**, *16*, 1112–1116.
(5) Peiro, A. M.; Ravirajan, P.; Govender, K.; Boyle, D. S.; O'Brien, P.; Bradley, D. D. C.; Nelson, J.; Durrant, J. R. *J. Mater. Chem.* **2006**, *16*, 2088–2096.
(6) White, M. S.; Olson, D. C.; Shaheen, S. E.; Kopidakis, N.; Ginley, D. S. *Appl. Phys. Lett.* **2006**, *89*, 143517.
(7) Briseno, A. L.; Holcombe, T. W.; Boukai, A. I.; Garnett, E. C.; Shelton, S. W.; Frechet, J. M. J.; Yang, P. *Nano Lett.* **2010**, *10*, 334–340.
(8) Gonzales-Valls, I.; Lira-Cantu, M. *Energy Environ.* **2008**, *2*, 19–34.
(9) Zhang, F.; Xu, X.; Tang, W.; Zhang, J.; Zhuo, Z.; Wang, J.; Wang, J.; Xu, Z.; Wang, Y. *Sol. Energy. Mater. Sol. Cells* **2011**, *95*, 1785–1799.
(10) Coakley, K. M.; Liu, Y.; McGehee, M. D.; Frindell, K. L.; Stucky, G. D. *Adv. Funct. Mater.* **2003**, *13*, 301–306.
(11) Kroeze, J. E.; Savenije, T. J.; Vermeulen, M. J. W.; Warman, J. M. *J. Phys. Chem. B* **2003**, *107*, 7696–7705.
(12) Piris, J.; Kopidakis, N.; Olson, D. C.; Shaheen, S. E.; Ginley, D. S.; Rumbles, G. *Adv. Funct. Mater.* **2007**, *17*, 3849–3857.
(13) Ameri, T.; Dennier, G.; Waldauf, C.; Denk, P.; Forberich, K.; Scharber, M. C.; Brabec, C. J.; Hinger, K. *J. Appl. Phys.* **2008**, *103*, 084506.
(14) Takanezawa, K.; Hirota, K.; Wei, Q.-S.; Tajima, K.; Hashimoto, K. *J. Phys. Chem. C* **2007**, *111*, 7218–7223.
(15) Umeda, T.; Hashimoto, Y.; Mizukami, H.; Shirakawa, T.; Fujii, A.; Yoshino, K. *Synth. Met.* **2005**, *152*, 93–96.
(16) Shankar, K.; Mor, G. K.; Prakasam, H. E.; Varghese, O. K.; Grimes, C. A. *Langmuir* **2007**, *23*, 12445–12449.
(17) Waldauf, C.; Morana, M.; Denk, P.; Schilinsky, P.; Coakley, K. M.; Choulis, S. A.; Brabec, C. J. *Appl. Phys. Lett.* **2006**, *89*, 233517.
(18) Kudo, N.; Honda, S.; Shimazaki, Y.; Ohkita, H.; Ito, S.; Benten, H. *Appl. Phys. Lett.* **2007**, *90*, 183513.

(19) Yang, C.; Kim, J. Y.; Cho, S.; Lee, J. K.; Heeger, A. J.; Wudl, F. *J. Am. Chem. Soc.* **2008**, *130*, 6444−6450.
(20) Hau, S. K.; Yip, H.-L.; Acton, O.; Baek, N. S.; Ma, H.; Jen, A. K.-Y. *J. Mater. Chem.* **2008**, *18*, 5113−5119.
(21) Hau, S. K.; Cheng, Y.-J.; Yip, H.-L.; Zhang, Y.; Ma, H.; Jen, A. K.-Y. *ACS Appl. Mater. Interfaces* **2010**, *2*, 1892−1902.
(22) Hsieh, C.-H.; Cheng, Y.-J.; Li, P.-J.; Chen, C.-H.; Dubosc, M.; Liang, R.-M.; Hsu, C.-S. *J. Am. Chem. Soc.* **2010**, *132*, 4887−4893.
(23) Chen, C.-T.; Hsu, F.-C.; Kuan, S.-W.; Chen, Y.-F. *Sol. Energy. Mater. Sol. Cells* **2011**, *95*, 740−744.
(24) Ravirajan, P.; Peiro, A. M.; Nazeeruddin, M. K.; Graetzel, M.; Bradley, D. D. C.; Durrant, J. R.; Nelson, J. *J. Phys. Chem. B* **2006**, *110*, 7635−7639.
(25) Goh, C.; Scully, S.; McGehee, M. D. *J. Appl. Phys.* **2007**, *101*, 114503.
(26) Lin, Y.-Y.; Chu, T.-H.; Li, S.-S.; Chuang, C.-H.; Chang, C.-H.; Su, W.-F.; Chang, C.-P.; Chu, M. W.; Chen, C.-W. *J. Am. Chem. Soc.* **2009**, *131*, 3644−3649.
(27) Said, A. J.; Poize, G.; Martini, C.; Ferry, D.; Marine, W.; Giorgio, S.; Fages, F.; Hocq, J.; Boucle, J.; Nelson, J.; Durrant, J. R.; Ackermann, J. *J. Phys. Chem. B* **2010**, *114*, 11273−11278.
(28) Zhu, R.; Jiang, C.-Y.; Liu, B.; Ramakrishna, S. *Adv. Mater.* **2009**, *21*, 994−1000.
(29) Lloyd, M. T.; Prasankumar, R. P.; Sinclair, M. B.; Mayer, A. C.; Olson, D. C.; Hsu, J. W. P. *J. Mater. Chem.* **2009**, *19*, 4609−4614.
(30) Kruger, J.; Bach, U.; Gratzel, M. *Adv. Mater.* **2000**, *12*, 447−451.
(31) Tian, X.; Xu, J.; Xie, W. *J. Phys. Chem. C* **2010**, *114*, 3973−3980.
(32) Liu, Y.; Scully, S. R.; McGehee, M. D.; Liu, J.; Luscombe, C. K.; Frechet, J. M. J.; Shaheen, S. E.; Ginley, D. S. *J. Phys. Chem. B* **2006**, *110*, 3257−3261.
(33) Liu, B.; Aydil, E. S. *J. Am. Chem. Soc.* **2009**, *131*, 3985−3990.
(34) Kavan, L.; Gratzel, M.; Gilbert, S. E.; Klemenz, C.; Scheel, H. J. *J. Am. Chem. Soc.* **1996**, *118*, 6716−6723.
(35) Imanishi, A.; Tsuji, E.; Nakato, Y. *J. Phys. Chem. C* **2007**, *111*, 2128−2132.
(36) Guan, Z.-L.; Kim, J. K.; Wang, H.; Jayye, C.; Fischer, D. A.; Loo, Y.-L.; Kahn, A. *Org. Elec.* **2010**, *11*, 1779−1785.
(37) Murphy, A. R.; Liu, J.; Luscombe, C. K.; Kavulak, D.; Frechet, J. M. J.; Kline, R. J.; McGehee, M. D. *Chem. Mater.* **2005**, *17*, 4892−4899.
(38) Al-Ibrahim, M.; Roth, H.-K.; UZhokhavets, U.; Gobsch, G.; Sensfuss, S. *Sol. Energy. Mater. Sol. Cells* **2005**, *85*, 13−20.
(39) Roberts, L. W.; Schuster, G. B. *Org. Lett.* **2004**, *6*, 3813−3816.
(40) Guldi, D. M.; Hungerbuhler, H.; Asmus, K.-D. *J. Phys. Chem.* **1995**, *99*, 9380−9385.
(41) Ross, R. B.; Cardona, C. M.; Guldi, D. M.; Sankaranarayanan, S. G.; Reese, M. O.; Kopidakis, N.; Peet, J.; Walker, B.; Bazan, G.; Van Keuren, E.; Holloway, B. C.; Drees, M. *Nat. Mater.* **2009**, *8*, 208−212.
(42) Guldi, D. M.; Asmus, K.-D. *J. Phys. Chem. A* **1997**, *101*, 1472−1481.
(43) Hoppe, H.; Glatzel, T.; Niggemann, M.; Hinsch, A.; Lux-Steiner, M. C.; Sariciftci, N. S. *Nano Lett.* **2005**, *5*, 269−274.
(44) van Duren, J. K. J.; Yang, X.; Loos, J.; Bulle-Lieuwma, C. W. T.; Sieval, A.; Hummelen, J. C.; Janssen, R. A. J. *Adv. Funct. Mater.* **2004**, *14*, 425−434.
(45) Boudon, C.; Gisselbrecht, J.-P.; Gross, M.; Isaacs, L.; Anderson, H. L.; Faust, R.; Diederich, F. *Helv. Chim. Acta* **1995**, *78*, 1334−1344.
(46) Cahen, D.; Hodes, G.; Gratzel, M.; Guillemoles, J. F.; Riess, I. *J. Phys. Chem. B* **2000**, *104*, 2053−2059.
(47) Pavlishchuk, V. V.; Addison, A. W. *Inorg. Chim. Acta* **2000**, *298*, 97−102.
(48) Bredas, J. L.; Silbey, R.; Boudreaux, D. S.; Chance, R. R. *J. Am. Chem. Soc.* **1983**, *105*, 6555−6559.
(49) Beuerle, F.; Chronakis, N.; Hirsch, A. *Chem. Commun.* **2005**, 3676−3678.
(50) Cormier, R. A.; Connolly, J. S.; Pelter, L. S. *Synth. Commun.* **1992**, *22*, 2155−2164.
(51) Riley, R. G.; Silverstein, R. M.; Katzenellenbogen, J. A.; Lenox, R. S. *J. Org. Chem.* **1974**, *39*, 1957−1958.
(52) Friedman, L.; Fishel, D. L.; Shechter, H. *J. Org. Chem.* **1965**, *30*, 1453−1457.
(53) Ohyama, M.; Kozuka, H.; Yoko, T. *Thin Solid Films* **1997**, 78−85.
(54) Kotov, M.; Hodes, G. *J. Mater. Chem.* **2009**, *19*, 3847−3854.
(55) Ruhle, S.; Greenstein, M.; Chen, S.-G.; Merson, A.; Pizem, H.; Sukenik, C. S.; Cahen, D.; Zaban, A. *J. Phys. Chem. B* **2005**, *109*, 18907−18913.
(56) Johansson, E. M. J.; Scholin, R.; Siegbahn, H.; Hagfeldt, A.; Rensmo, H. *Chem. Phys. Lett.* **2011**, *515*, 146−150.
(57) Braun, S.; Salaneck, W. R.; Fahlman, M. *Adv. Mater.* **2009**, *21*, 1450−1472.
(58) Parker, R. A. *Phys. Rev.* **1961**, *124*, 1719−1722.
(59) Ozgur, U.; Alivov, Y. I.; Liu, C.; Teke, A.; Reshchikov, M. A.; Dogan, S.; Avrutin, V.; Cho, S. J.; Morkoc, H. *J. Appl. Phys.* **2005**, *98*, 041301.
(60) Yamaji, M.; Takehira, K.; Itoh, T.; Shizuka, H.; Tobita, S. *Phys. Chem. Chem. Phys.* **2001**, *3*, 5470−5474.
(61) Yamaji, M.; Itoh, T.; Tobita, S. *Photochem. Photobiol. Sci.* **2002**, *1*, 869−876.
(62) Badger, G. M. *Quart. Rev. (London) Biol.* **1951**, *5*, 155.
(63) Berhe, S. A.; Zhou, J. Y.; Youngblood, W. J.
(64) Jensen, R. A.; Ryswyk, H. V.; She, C.; Szarko, J. M.; Chen, L. X.; Hupp, J. T. *Langmuir* **2010**, *26*, 1401−1404.
(65) Horiuchi, H.; Katoh, R.; Hara, K.; Yanagida, M.; Murata, S.; Arakawa, H.; Tachiya, M. *J. Phys. Chem. B* **2003**, *107*, 2570−2574.
(66) Plank, N. O. V.; Howard, I.; Rao, A.; Wilson, M. W. B.; Ducati, C.; Mane, R. S.; Bendall, J. S.; Louca, R. R. M.; Greenham, N. C.; Miura, H.; Friend, R. H.; Snaith, H. J.; Welland, M. E. *J. Phys. Chem. C* **2009**, *113*, 18515−18522.
(67) Quintana, M.; Edvinsson, T.; Hagfeldt, A.; Boschloo, G. *J. Phys. Chem. C* **2007**, *111*, 1035−1041.
(68) van der Berg, R. A.; Blom, P. W. M.; Cillessen, J. F. M.; Wolf, R. M. *Appl. Phys. Lett.* **1995**, *66*, 697−699.
(69) Li, J.; Olszta, M.; Dickey, C. *Microsc. Microanal.* **2007**, *13*, 1002−1003.
(70) van Daal, H. J. *J. Appl. Phys.* **1968**, *39*, 4467.